Nonlinear solutions for the steady state oscillations of a clamped-free rotating beam

González-Carbajal, J.[a,*], Rincón-Casado, A.[b], García-Vallejo, D.[a] and Domínguez, J.[a]

[a]Department of Mechanical Engineering and Manufacturing, Universidad de Sevilla, 41092 Seville, Spain
[b]Department of Mechanical Engineering and Industrial Design, University of Cadiz, 11519 Puerto Real, Spain

ARTICLE INFO

Keywords:
rotating beam
multiple time scales
absolute nodal coordinate formulation
nonlinear oscillation
Frobenius method

ABSTRACT

The rotating beam problem has been extensively used as a benchmark for testing nonlinear finite element implementations. The remarkable characteristic of this benchmark is the coupling between axial a transverse deformations due to the centrifugal forces. The rotating beam dynamics exhibits a centrifugal stiffening effect that can only be captured either by including a kinematic coupling between axial and transverse deformation or by using a nonlinear description of the elastic forces. This paper presents simplified models of the rotating beam that capture the centrifugal stiffening effect due to the inclusion of an axial to transverse kinematic coupling of the beam centreline. The simplified models allow a discussion on their accuracy and a meaningful analysis of the nonlinear oscillations present in the steady state rotation. The results of the simplified models are compared to finite element solutions obtained by using the absolute nodal coordinate formulation and a commercial FEM code.

1. Introduction

Rotating beams are found in many applications including helicopter rotor blades, wind turbine blades and space booms. The large rotation of such flexible structures induces nonlinear oscillations even when their amplitude is not necessarily large. From a design point of view, the knowledge of the effects that take place in such situations is of high interest. In addition, having simple models that resemble the behaviour of a detailed finite element model might help designer's work.

Due to its nonlinear nature, the rotating beam problem has been utilized as a benchmark in the development of flexible multibody formalisms. Therefore, the advance in the understanding of this classical problem and the possibility of having a simple model that represents the main features of this benchmark may be of interest for researchers in the field of Flexible Multibody Systems Dynamics. The benchmark consists of a cantilever beam, as the one in Fig. 1, which is rotating in a plane perpendicular to the direction of gravity forces. The clamped end is forced to rotate at an angular velocity $\dot{\theta}(t)$ that is increased from zero to a constant value, ω. When the beam achieves the constant angular velocity, it remains oscillating since no dissipative forces are included.

In the dynamic simulation, the beam is subject to a prescribed rotation according to:

$$\theta(t) = \begin{cases} \dfrac{\omega}{T}\left(\dfrac{t^2}{2} + \dfrac{T^2}{4\pi^2}\left(\cos\dfrac{2\pi t}{T} - 1\right)\right) & t < T \\ \omega\left(t - \dfrac{T}{2}\right) & t \geq T \end{cases}, \tag{1}$$

where ω is the steady state value of the angular velocity and T is the time elapsed from rest to steady state rotation of the clamped end.

According to the literature (García-Vallejo, Sugiyama and Shabana, 2005a), when the previous beam is modelled by using only one substructure, the elastic forces are formulated according to the linear theory of elasticity, and the final steady value of the angular velocity is larger than the first natural frequency of a non rotating cantilever beam, the free end transverse displacement grows without bound showing an unstable oscillation, which clearly does not correspond

*Corresponding author
jgcarbajal@us.es (G. J.); alejandro.rincon@uca.es (R. A.); dgvallejo@us.es (G. D.); jaime@us.es (D. J.)
ORCID(s): 0000-0002-1379-0406 (G. J.); 0000-0001-9625-1880 (R. A.); 0000-0002-2319-2688 (G. D.); 0000-0002-0491-7911 (D. J.)

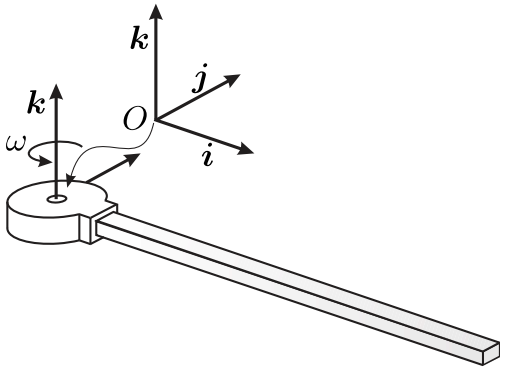

Figure 1: Rotating beam model.

to the real behaviour of the system. Valverde and García-Vallejo (Valverde and García-Vallejo, 2009) showed that using a substructuring approach the necessary nonlinear description can be successively incorporated by increasing the number of substructures. For any number of substructures, there will always be a critical value of the angular velocity for which the beam model behaves unstably. The value of the critical angular velocity depends on the co-rotational frame (pinned or tangent) used in each substructure. The critical angular velocity is due to the mathematical description, since it does not appear in fully nonlinear models where nonlinear elasticity effects are accounted for, see García-Vallejo et al. (García-Vallejo et al., 2005a; García-Vallejo, Sugiyama and Shabana, 2005b).

The source of the nonlinearities in the rotating beam oscillations is twofold. First, the nonlinear nature of the curvature definition, which is needed for the formulation of the elastic forces of the rotating beam model, introduces a nonlinear behaviour to the beam oscillations. In this respect, the works of Babilio and Lenci (2017) and Lenci, Clementi and Rega (2017) have studied in detail the nonlinear effect caused by the different curvature definitions (geometrical or mechanical) both in Euler-Bernouilli and Timoshenko beams. Second, the nonlinear effects caused by the inertial forces, that for the case of rotating beams can be separated in two causes: i) the coupling between the horizontal and rotary inertial terms with the transverse oscillations as explained by Atluri (1973) and Lenci and Rega (2016) and ii) the coupling of the large beam rotation and deformation, which has been a matter of research in the field of flexible multibody system, see for example (Mayo, Dominguez and Shabana, 1995). Recently, Arvin, Arena and Lacarbonara (2020) investigated the free oscillation and the parametric resonance of rotating beams including nonlinearities due to Coriolis forces in the coupling between lagging to axial deformation. They studied in detail the effect of the rotational velocity and the damping on the nonlinearities appearing in this kind of beams. Zhang, Ding and Chen (2020) studied the resonances of rotating beam models having a pre-deformed configuration. Their model, which included quadratic and cubic nonlinear terms, shows three-to-one internal resonances. They also studied the stability regions of their solutions. Warminski, Kloda and Lenci (2020) obtained the partial differential equations of a rotating beam with tip mass including nonlinear curvature effects and studied the nonlinear resonance of the solution at certain frequency regimes, considering the effect of some constructive parameters. Bekhoucha, Rechak, Duigou and Cadou (2016) studied the backbone curves for the first lagging and flapping modes of a centrifugally stiffened cantilever beam using Galerkin's method in combination with the harmonic balance method. Tian, Su, Zhou and Hua (2018) used a variational method to study the transient and free nonlinear vibration of rotating beams accounting for Coriolis effects and the coupling of bending-stretching, bending-twist and twist-stretching.

Among the many available techniques (Galerkin's method, harmonic balance, averaging, etc.) that can be used to obtain solutions for nonlinear oscillating systems, the multiple time scale method is a well-acknowledge perturbation method that is frequently used, see Thomsen (2003). This method generates an approximate solution as a series of nonlinear harmonic terms and due to the use of various time scales it avoids the appearance of secular terms. For instance, it has been used in conjunction with the nonlinear normal mode's method for the analysis of non linear oscillations of beams (Nayfeh and Nayfeh, 1994; Nayfeh, Chin and Nayfeh, 1995; Kloda, Lenci and Warminski, 2018; Rincón-Casado, González-Carbajal, García-Vallejo and Domínguez, 2021).

Linear modes of rotating beams have been a matter of research for a long time. Among other, the early works of Hodges (1979) in non-uniform beams with discontinuities and the work of Wright, Smith, Thresher and Wang (1982)

also for the mode shape representation of rotating beams with linearly varying properties are well acknowledged. More recently, Banerjee (2000); Banerjee and Jackson (2013); Banerjee and Kennedy (2014) studied the free vibration of uniform and non-uniform rotating beams based on the so-called dynamic stiffness method. Tsai, Lin, Zhou and Hsiao (2011) studied the steady state deformation and its influence on the free vibration of rotating beams by using a co-rotational finite element method in combination with the floating frame method. Tang, Li, Wu and Lee (2015) studied the influence of constructive parameters, including the rotary inertia, in the natural frequencies of power-law varying width and height tapered rotating beams. Kim, Hee Yoo and Chung (2013) proposed a method for vibration analysis of rotating beams based on von Karman strain definition and computed the natural frequencies and time responses. The natural frequencies of functionally graded tapered beams were studied by Rajasekaran (2013) by using the so-called differential transformation and differential quadrature methods.

The objective of this paper is to develop simple models and their solutions that account for cubic nonlinearities present in rotating beams. The main features of such simplified models are presented in an incremental manner, allowing to identify their effect on the solution. In particular, this paper makes emphasis on the importance of modelling the extensibility of the rotating beam and the selection of an adequate shape function when the assumed mode method is used. A detailed well-acknowledged finite element method based on the Absolute Nodal Coordinate Formulation (ANCF) is used for comparison to the analytical results, leading to a numerical validation of the analytical models.

The structure of this work is as follows. In Section 2 a precise ANCF finite element model is presented and the main nonlinear effects found in its results are shown. Section 3 presents a simplified model with up to cubic nonlinearities of the rotating beam and its solution through the use of the multiple time scales technique. Section 4 presents a simplified approach that allows one to incorporate the elongation of the rotating beam due to the centrifugal forces and comments the effect of such consideration on the solution. Section 5 shows a procedure to obtain and add the exact vibration mode of the rotating beam into the equations of motion and shows the nonlinear solutions obtained subsequently. Section 6 compares the results of the ANCF finite element model to the different analytical solutions to investigate the accuracy and influence of both the shape function choice and the effect of the beam axial elongation. Finally, summary and conclusions drawn from the analysis are included in Section 7.

2. A nonlinear planar finite element model of the rotating beam based on the Absolute Nodal Coordinate Formulation

In this work a fully nonlinear flexible multibody model of the rotating beam based on the ANCF will be used. The model is built with the quadratic three-noded beam elements developed by García-Vallejo, Mikkola and Escalona (2007) shown in Fig. 2. In the figure, the transverse slope vectors and the position vector of nodes i, j and k of the element are shown. These vectors are all described in the inertial frame.

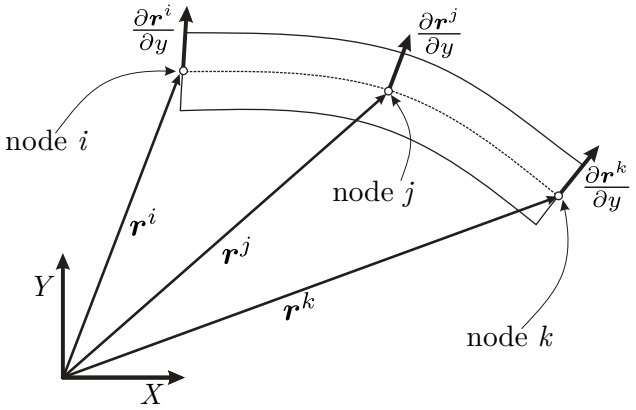

Figure 2: Three-noded shear locking free beam element developed by García-Vallejo et al. (García-Vallejo et al., 2007).

An arbitrary element nodal coordinate vector can be written in matrix form as follows

$$\boldsymbol{e} = \left(\boldsymbol{r}^{iT},\ \frac{\partial \boldsymbol{r}^{iT}}{\partial y},\ \boldsymbol{r}^{jT},\ \frac{\partial \boldsymbol{r}^{jT}}{\partial y},\ \boldsymbol{r}^{kT},\ \frac{\partial \boldsymbol{r}^{kT}}{\partial y} \right)^T \tag{2}$$

where the number of the element is omitted for simplicity. The position vector of an arbitrary point in the element can be written as follows

$$\boldsymbol{r} = \boldsymbol{S}(x, y)\,\boldsymbol{e} \tag{3}$$

where x and y are the longitudinal and transversal parameters of the element, respectively, and $\boldsymbol{S}(x, y)$ is the following element shape function matrix

$$\boldsymbol{S}(x, y) = \left(s_1(x, y)\,\boldsymbol{I},\ s_2(x, y)\,\boldsymbol{I},\ s_3(x, y)\,\boldsymbol{I},\ s_4(x, y)\,\boldsymbol{I},\ s_5(x, y)\,\boldsymbol{I},\ s_6(x, y)\,\boldsymbol{I}\right) \tag{4}$$

where $\boldsymbol{I}$ is a 2×2 identity matrix and $s_j(x, y)$ $(j = 1, 2...6)$ are as follows

$$s_1(x, y) = 1 - 3\left(\frac{x}{l_e}\right) + 2\left(\frac{x}{l_e}\right)^2, \qquad s_2(x, y) = l_e\left(\frac{y}{l_e}\right)\left(1 - 3\left(\frac{x}{l_e}\right) + 2\left(\frac{x}{l_e}\right)^2\right) \tag{5}$$

$$s_3(x, y) = 4\left(\frac{x}{l_e}\right) - 4\left(\frac{x}{l_e}\right)^2, \qquad s_4(x, y) = l_e\left(\frac{y}{l_e}\right)\left(4\left(\frac{x}{l_e}\right) - 4\left(\frac{x}{l_e}\right)^2\right) \tag{6}$$

$$s_5(x, y) = -\left(\frac{x}{l_e}\right) + 2\left(\frac{x}{l_e}\right)^2, \qquad s_6(x, y) = l_e\left(\frac{y}{l_e}\right)\left(-\left(\frac{x}{l_e}\right) + 2\left(\frac{x}{l_e}\right)^2\right) \tag{7}$$

being l_e the length of the element in the reference configuration.

The element equations of motion can be obtained for instance by using Lagrange equations. The kinetic energy can be calculated directly given that the velocity of one point is proportional to the time derivative of the nodal coordinate vector as follows:

$$T = \frac{1}{2}\int_{\Phi_0(\Omega)} \rho\left(\dot{\boldsymbol{r}}^T\dot{\boldsymbol{r}}\right) dV_0 = \frac{1}{2}\dot{\boldsymbol{e}}^T\boldsymbol{M}_e\dot{\boldsymbol{e}} \tag{8}$$

where ρ is the element mass density in the reference configuration, $\Phi_0(\Omega)$ is the element volume in the reference configuration and Ω is the volume of the element in an undistorted configuration. The element mass matrix, $\boldsymbol{M}_e$ is obtained as follows:

$$\boldsymbol{M}_e = \int_{\Phi_0(\Omega)} \rho\boldsymbol{S}^T\boldsymbol{S}\,\mathrm{d}V_0 = \int_{\Omega} \rho\boldsymbol{S}^T\boldsymbol{S}\left|\boldsymbol{J}_0\right|\mathrm{d}V \tag{9}$$

where $\left|\boldsymbol{J}_0\right|$ is the Jacobian of the mapping from the undistorted to the reference configurations. The element elastic forces are obtained by derivation of the stored elastic deformation energy using the Green-Lagrange deformation tensor as shown next:

$$\boldsymbol{\varepsilon} = \frac{1}{2}\left(\boldsymbol{J}^T\boldsymbol{J} - \boldsymbol{I}\right) \tag{10}$$

where $\boldsymbol{J}$ is the deformation gradient calculated as the derivative of the position vector with respect to the position vector in the undistorted configuration as follows:

$$\boldsymbol{J} = \frac{\partial\boldsymbol{r}}{\partial\boldsymbol{r}_0} \tag{11}$$

being $\boldsymbol{r}_0$ the position vector of a point in the reference configuration. The elastic deformation energy is computed as the integral of the product of the Green-Lagrange deformation tensor, $\boldsymbol{\varepsilon}$, and the second Piola-Kirchoff stress tensor (Omar and Shabana, 2001), $\boldsymbol{\sigma}$, on the element volume. Again, the mapping from the undistorted to the reference configurations can be used as follows:

$$U_e = \frac{1}{2}\int_{\Phi_0(\Omega)} \boldsymbol{\sigma}\cdot\boldsymbol{\varepsilon}\,\mathrm{d}V_0 = \frac{1}{2}\int_{\Omega} \boldsymbol{\sigma}\cdot\boldsymbol{\varepsilon}\left|\boldsymbol{J}_0\right|\,\mathrm{d}V \tag{12}$$

where $\cdot$ indicates the tensor internal product. According to García-Vallejo et al. (2007), a two-point Gauss–Legendre reduced numerical integration is used to avoid shear locking due to excessive shear strain energy.

To impose the beam rotation, two angular constraints are used. Therefore, the set of equations of motion is as follows:

$$\begin{aligned} \boldsymbol{M}\ddot{\boldsymbol{x}} + \boldsymbol{C}_{\boldsymbol{x}}{}^{T}\lambda &= \boldsymbol{Q}\left(\boldsymbol{x}, \dot{\boldsymbol{x}}\right) \\ \boldsymbol{C}\left(\boldsymbol{x}, t\right) &= \boldsymbol{0} \end{aligned} \tag{13}$$

where $\boldsymbol{M}$ is the global mass matrix, $\boldsymbol{x}$, $\dot{\boldsymbol{x}}$ and $\ddot{\boldsymbol{x}}$ are the system position, velocity and acceleration vectors, $\boldsymbol{C}_{\boldsymbol{x}}$ is the constraint Jacobian matrix, λ is the Lagrange multipliers vector, $\boldsymbol{Q}\left(\boldsymbol{x}, \dot{\boldsymbol{x}}\right)$ is the generalized force vector due to elastic, centrifugal and Coriolis forces and $\boldsymbol{C}\left(\boldsymbol{x}, t\right)$ is the constraints vector

$$\boldsymbol{C}\left(\boldsymbol{x}, t\right) = \begin{pmatrix} x_3 + \sin\left(\theta\left(t\right)\right) \\ x_4 - \cos\left(\theta\left(t\right)\right) \end{pmatrix} \tag{14}$$

being x_3 and x_4 the components of the gradient vector $\dfrac{\partial \boldsymbol{r}}{\partial y}$ at the clamped node.

Several authors have studied this problem with different parameter values, while this fact has no influence on the salient features of this benchmark problem. In this paper, the beam is assumed to have a cross-sectional area of $7.299{\cdot}10^{-5}$ m^2, a second moment of the area of $8.214{\cdot}10^{-9}$ m^4, a Young modulus of $6.895{\cdot}10^{10}$ N/m^2, a mass density of 2767 kg/m^3 and a length of 8 m. This set of values has been taken from previous work for the sake of comparison (Valverde and García-Vallejo, 2009).

Figure 3 shows the transverse displacement of the beam's free end obtained with three different finite element meshes. It is noteworthy that the results show a fast convergence and that, due to the nonlinear description of the elastic forces, even one element is able to behave stably. As demonstrated by García-Vallejo et al. (2005a), if a linear elastic model based on the floating frame of reference formulation is used with the same set of parameters an unstable (unbounded) solution would be obtained. One can also see that, due to the absence of damping in the model, once the steady angular velocity is achieved, the transverse displacement of the beam tip shows oscillations, see the shaded area in Fig. 3. Such oscillations, which are highly dependent on the angular velocity, ω, and on the time elapsed from rest to the steady angular rotation, T, have been less studied in the literature and are the focus of this work.

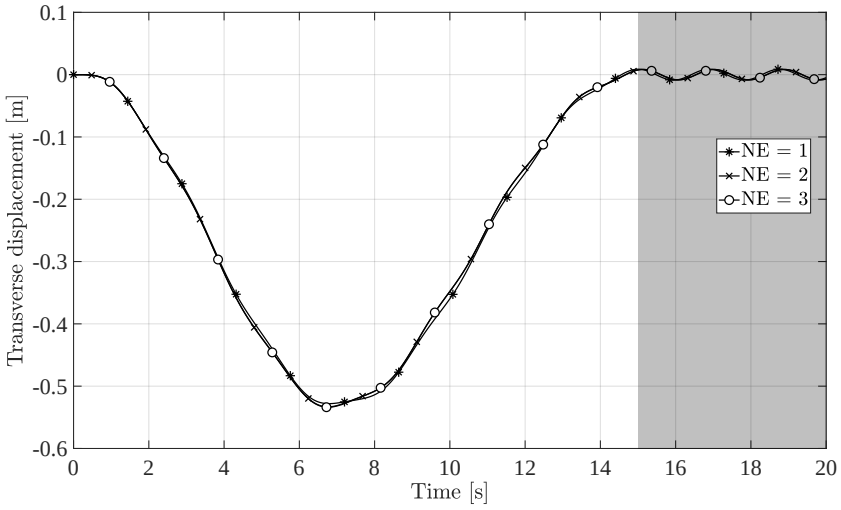

Figure 3: Transverse displacement of the free end of three ANCF models with 1, 2 and 3 elements, respectively, for $\omega = 4$ rad/s and $T = 15$ s.

In order to appreciate the steady nonlinear oscillations of the tip of the beam, the following non-dimensional

variables are defined:

$$\bar{q} = \frac{q}{q_0}, \quad \bar{\dot{q}} = \frac{\dot{q}}{\dot{q}_0} \tag{15}$$

where q is the transverse displacement of the beam tip, $\dot{q}$ is its time derivative and q_0 and $\dot{q}_0$ are a reference displacement and a reference velocity for the adimensionalization. Using the rotating unit vectors $\boldsymbol{i}$ and $\boldsymbol{j}$ depicted in Fig. 1, one can obtain

$$q = \boldsymbol{j} \cdot \boldsymbol{r_L} \rightarrow \dot{q} = \boldsymbol{j} \cdot \dot{\boldsymbol{r}}_{\boldsymbol{L}} - \dot{\theta}\, \boldsymbol{i} \cdot \boldsymbol{r_L} \tag{16}$$

where $\boldsymbol{r_L}$ is the position vector of the beam tip. The values q_0 and $\dot{q}_0$ are selected considering that the magnitude of the oscillations depends on the maximum inertial force during the acceleration. For this reason, the maximum angular acceleration ($2\omega/T$) according to Eq. (1) is used to calculate a reference inertial force, which divided by a representative stiffness leads to q_0. Finally, $\dot{q}_0$ is obtained dividing q_0 by a representative value of the linear natural frequency. That is to say,

$$q_0 = \frac{m(\omega/T)L}{\dfrac{EI}{L^3} + m\omega^2} = \frac{m\omega L^4}{T\left(EI + m\omega^2 L^3\right)} \tag{17}$$

$$\dot{q}_0 = \frac{q_0}{\sqrt{\dfrac{EI}{mL^3} + \omega^2}} = \frac{\omega L}{T}\sqrt{\frac{mL^3}{EI + m\omega^2 L^3} + \omega^2} \tag{18}$$

The use of the previous normalization allows a clearer representation of the beam's tip oscillation in the phase space as shown in Fig. 4a) and b), since otherwise the sizes of the close orbits are too different. In Fig. 4a) the effect of the amplitude of the oscillations is varied by reducing the acceleration time, T. As can be seen the shape of the orbits is not elliptical as in linear systems. In particular, comparing the shapes of the orbits for T= 1.5 s and T= 2 s the distortion of the shape is evident. Figure 4b) shows the effect of the steady angular velocity for a fixed acceleration time, T. While the shapes of the orbits are apparently similar to a linear behaviour it can be shown that the fact that they have different horizontal to vertical axes proportions is the results of a nonlinear oscillation.

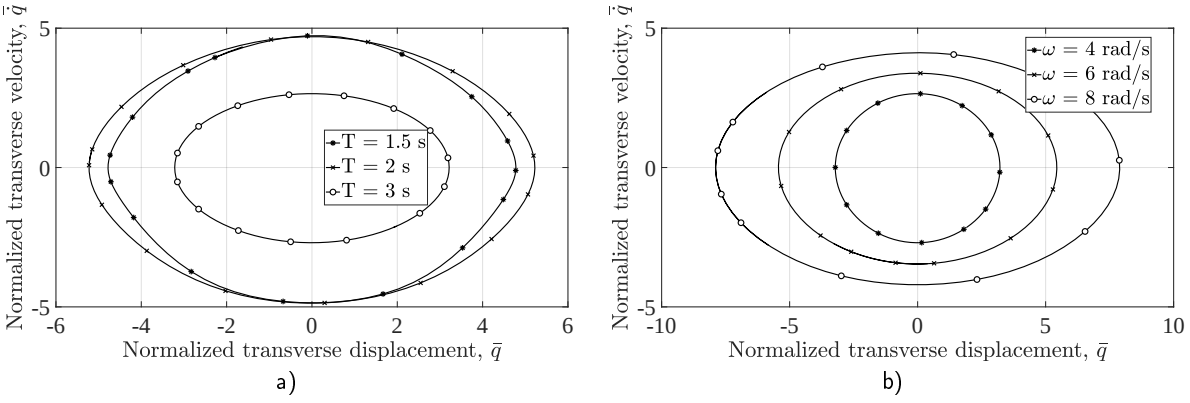

Figure 4: Phase space representation of the normalized displacement, $\bar{q}$, in models with 3 ANCF beam elements: a) $\omega = 4$ rad/s, T = 1.5, 2 and 3 s; b) $T = 3s$, ω = 4, 6 and 8 rad/s

Figure 5 shows how the nonlinear frequency of the oscillations depends on the oscillation amplitude for different values of the angular velocity, ω. The results of the ANCF model are plotted as points in the graph while the lines are mean square approximations of such point values, showing a nearly quadratic dependence of the ratio ω_{NL}/ω_n on the normalized oscillation amplitude, $a = q/L$. Here ω_n is the natural frequency obtained with the ANCF model in case of small oscillations.

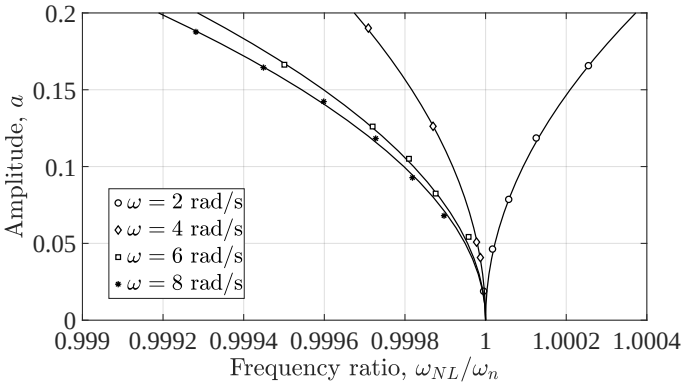

Figure 5: Frequency-amplitude relation (backbone curve) for different values of ω.

The investigation of the previous nonlinear behaviours as function of the acceleration time, that is the steady oscillation amplitude, and the steady angular velocity is the objective of this paper. Since analysing the behaviour of the system with a finite element model may be complicated, the next section presents simplified models of the rotating beam which allow the interpretation of the aforementioned nonlinear effects.

3. A simplified model for nonlinear free oscillations of an inextensible rotating beam

In this section, an analytical model of the flexible beam shown in Fig. 6 rotating at constant angular velocity is developed. The model should capture the principal features of the ANCF model described before during the steady oscillation, shaded area in Fig. 3.

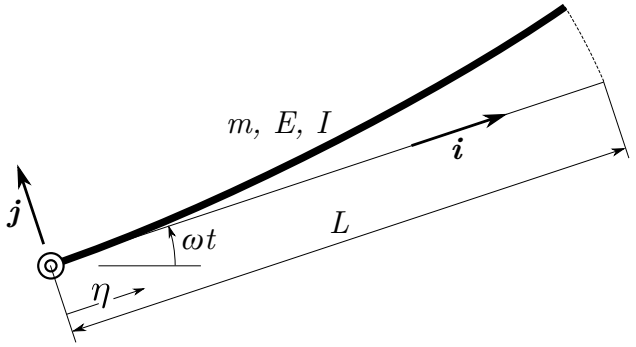

Figure 6: Clamped-free beam rotating at constant angular velocity.

In order to have a relatively simple model, the deformation will be described by using the Rayleigh method by selecting an appropriate assumed shape function for transverse deformation. It will be assumed that the cross-section will remain planar after deformation and no shear deformation is accounted for. The bending deformation will be allowed to be moderately large and therefore second order terms are retained. In addition, the beam is assumed to be inextensible. This last assumption is used to obtain a shape function for the axial displacement.

Figure 7 shows a sketch of the rotating beam model. According to the figure, it can be seen that the expression of the increment ds can be obtained as follows

$$\mathrm{d}s = \sqrt{(\mathrm{d}\eta + \mathrm{d}u)^2 + (\mathrm{d}v)^2} \tag{19}$$

where η is the axial position of an arbitrary point of the beam in its undeformed configuration, u and v are the axial and transverse displacements and s is an arc length parameter along the beam centreline for an arbitrary point. Dividing

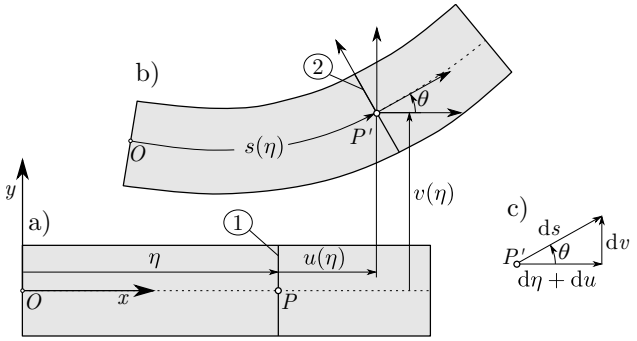

Figure 7: Sketch of a flexible beam: a) undeformed configuration; b) deformed configuration; and c) description of the beam centreline elongation.

the previous equation by dη leads to

$$s' = \sqrt{(1+u')^2 + (v')^2} = \sqrt{1 + 2u' + (u')^2 + (v')^2} \tag{20}$$

The beam centreline elongation s' will be approximated using the Taylor series of function $\sqrt{1+x}$ around $x = 0$ retaining second order terms

$$\sqrt{1+x} = 1 + \frac{1}{2}x - \frac{1}{8}x^2 + \mathcal{O}(x^3) \tag{21}$$

Assuming that $2u' + (u')^2 + (v')^2$ is small enough one can write

$$s' = 1 + \frac{1}{2}\left(2u' + (u')^2 + (v')^2\right) - \frac{1}{8}\left(2u' + (u')^2 + (v')^2\right)^2 + \mathcal{O}((u')^3) \tag{22}$$

what leads to

$$s' = 1 + u' + \cancel{\frac{1}{2}(u')^2} + \frac{1}{2}(v')^2 - \cancel{\frac{1}{8}4(u')^2} + \mathcal{O}((u')^3) = 1 + u' + \frac{1}{2}(v')^2 + \mathcal{O}((u')^3) \tag{23}$$

and finally

$$s' \approx 1 + u' + \frac{1}{2}(v')^2 \tag{24}$$

Assuming that the centreline is inextensible ($s' - 1 = 0$) one can write

$$u' = -\frac{1}{2}(v')^2 \tag{25}$$

Using Rayleigh's discretization method, the transverse displacement of an arbitrary point in the beam can be written as

$$v(\eta, t) = \varphi_v(\eta)\, q(t) \tag{26}$$

where $\varphi_v(\eta)$ is an assumed shape function that fulfils $\varphi_v(L) = 1$ as well as the beam's boundary conditions and q represents the transverse displacement of the beam's tip. Using Eq. (25) one can obtain

$$u(\eta, t) = \int_0^\eta -\frac{1}{2}\left(\frac{\mathrm{d}v(\xi)}{\mathrm{d}\xi} q(t)\right)^2 \mathrm{d}\xi = \varphi_u(\eta)\, q^2(t) \tag{27}$$

that leads to

$$\varphi_u(\eta) = \int_0^\eta -\frac{1}{2}\left(\frac{\mathrm{d}\varphi_v(\xi)}{\mathrm{d}\xi}\right)^2 \mathrm{d}\xi \tag{28}$$

Using the previous shape functions, the position vector of an arbitrary point in the beam can be found as

$$\boldsymbol{r} = r_x \boldsymbol{i} + r_y \boldsymbol{j} = \left(\eta + \varphi_u(\eta)\, q^2\right) \boldsymbol{i} + \varphi_v(\eta) q \boldsymbol{j} \tag{29}$$

Then, the velocity of such point is

$$\dot{\boldsymbol{r}} = \varphi_u(\eta)\, 2q\dot{q}\boldsymbol{i} + \left(\eta + \varphi_u(\eta)\, q^2\right) \omega \boldsymbol{j} + \varphi_v(\eta)\dot{q}\boldsymbol{j} - \varphi_v(\eta) q\omega \boldsymbol{i} \tag{30}$$

With the previous velocity vector, the kinetic energy is as follows

$$\begin{aligned} T = \frac{1}{2}\int_0^L \frac{m}{L}\left(\dot{r}_x^2 + \dot{r}_y^2\right)^2 \mathrm{d}\eta = \\ \frac{1}{2}\int_0^L \frac{m}{L}\left(\left(\varphi_u(\eta)\, 2q\dot{q} - \varphi_v(\eta) q\omega\right)^2 + \left(\left(\eta + \varphi_u(\eta)\, q^2\right)\omega + \varphi_v(\eta)\dot{q}\right)^2\right)\mathrm{d}\eta \end{aligned} \tag{31}$$

and the elastic energy as

$$V = \frac{1}{2}\int_0^L EI\kappa^2 \mathrm{d}\eta \tag{32}$$

where κ is the following nonlinear geometric description of the curvature (Berzeri and Shabana, 2000):

$$\kappa = \frac{\|\boldsymbol{r}'' \times \boldsymbol{r}'\|}{\|\boldsymbol{r}'\|^3} \tag{33}$$

The curvature definition can be simplified by using the non-extensibility assumption and neglecting terms of order greater than three in the coordinate q. This way, the square of the curvature can be written as follows

$$\kappa^2 = \left(\frac{\|\boldsymbol{r}'' \times \boldsymbol{r}'\|}{\|\boldsymbol{r}'\|^3}\right)^2 = \frac{\left(v'' + u'v'' - u''v'\right)^2}{\left(1 + (u')^2 + \cancel{2u' + (v')^2}\right)^3} \tag{34}$$

Considering that u' has second order in q, one can write

$$\kappa^2 = \left(\frac{\|\boldsymbol{r}'' \times \boldsymbol{r}'\|}{\|\boldsymbol{r}'\|^3}\right)^2 = \left(\varphi_v(\eta)'' q + \varphi_u'(\eta)\varphi_v''(\eta) q^3 - \varphi_u''(\eta)\varphi_v'(\eta) q^3\right)^2 \left(1 + \mathcal{O}\left(q^4\right)\right) \tag{35}$$

where the denominator has been approximated by using the Taylor series of the function $1/(1+x)$ with $x << 1$. Finally, Eq. (35) can be reduced to

$$\kappa^2 = \left(\frac{\|\boldsymbol{r}'' \times \boldsymbol{r}'\|}{\|\boldsymbol{r}'\|^3}\right)^2 = \left(\varphi_v''(\eta)\right)^2 q^2 + 2\left(\varphi_v''(\eta)\varphi_u'(\eta)\varphi_v''(\eta) - \varphi_v''(\eta)\varphi_u''(\eta)\varphi_v'(\eta)\right) q^4 + \mathcal{O}\left(q^6\right) \tag{36}$$

According to the previous development, the elastic energy will be approximated by the following expression

$$V = \frac{1}{2}\left(\int_0^L EI\left(\varphi_v''(\eta)\right)^2 \mathrm{d}\eta\right) q^2 + \left(\int_0^L EI\left(\left(\varphi_v''(\eta)\right)^2 \varphi_u'(\eta) - \varphi_v''(\eta)\varphi_u''(\eta)\varphi_v'(\eta)\right)\mathrm{d}\eta\right) q^4 \tag{37}$$

that will retain third order terms in the equation of motion. Then, the equation of motion of the steady rotation of the flexible beam would be obtained from Lagrange's equation

$$\frac{\mathrm{d}}{\mathrm{d}t}\left(\frac{\partial T}{\partial \dot{q}}\right) - \frac{\partial T}{\partial q} + \frac{\partial V}{\partial q} = 0 \tag{38}$$

Using the first linear bending mode of a cantilever beam as assumed shape function, $\varphi_v(\eta)$, computing its corresponding axial shape function, $\varphi_u(\eta)$, using Eq. (28) and the previous expressions for the kinetic and elastic energies, the following equation is obtained:

$$0.25m\ddot{q} + \left(3.0906\frac{EI}{L^3} + 0.048334m\omega^2\right) q + \left(2.5275\frac{EI}{L^5} - 0.14365\frac{m\omega^2}{L^2}\right) q^3 + 0.28730\frac{m}{L^2}\left(q\dot{q}^2 + q^2\ddot{q}\right) = 0 \tag{39}$$

Notice that the use of integer numbers in the equation is impossible due to the non-rational nature of the coefficients of the first theoretical linear mode of a cantilever beam. To analyse the influence of the different terms, the following definitions are used:

$$\omega_0 = 3.516\sqrt{\frac{EI}{mL^3}},\ \tau = \sqrt{\frac{EI}{mL^3}}t,\ x = \frac{q}{L},\ \frac{\mathrm{d}x}{\mathrm{d}\tau} = \frac{\dot{q}}{\sqrt{\frac{EI}{mL^3}}L},\ \frac{\mathrm{d}^2x}{\mathrm{d}\tau^2} = \frac{\ddot{q}}{\frac{EI}{mL^3}L},\ \Omega = \frac{\omega}{\omega_0}. \tag{40}$$

where ω_0 is the first natural frequency of the non-rotating cantilever beam (Shabana, 2019). With the previous definitions, Eq. (39) can be written as follows

$$\frac{\mathrm{d}^2x}{\mathrm{d}\tau^2} + \omega_n^2 x + g_1 x^3 + g_2\left(x\left(\frac{\mathrm{d}x}{\mathrm{d}\tau}\right)^2 + \frac{\mathrm{d}^2x}{\mathrm{d}\tau^2}x^2\right) = 0 \tag{41}$$

with

$$\omega_n^2 = 12.362 + 2.3901\Omega^2 \tag{42}$$

$$g_1 = 10.110 - 7.1034\Omega^2 \tag{43}$$

$$g_2 = 1.1492 \tag{44}$$

In order to simplify the notation, in what follows $\frac{\mathrm{d}x}{\mathrm{d}\tau}$ and $\frac{\mathrm{d}^2x}{\mathrm{d}\tau^2}$ are regarded as $\dot{x}$ and $\ddot{x}$, respectively. According to the coefficients of Eq. (41) both the nonlinearity due to the centrifugal forces and to the curvature contribute to the linear and cubic stiffness terms. However, it is remarkable that the centrifugal forces result in a hardening linear but a softening cubic terms. In addition, it is interesting that the nonlinear inertial terms ($x\dot{x}^2 + \ddot{x}x^2$) do not depend on the angular velocity, ω. Observe that if the term $\varphi_u(\eta)\,q^2$ is omitted in Eq. (29), following the previous procedure, one would arrive at the following linear equation

$$\frac{\mathrm{d}^2x}{\mathrm{d}\tau^2} + 12.362\left(1 - \Omega^2\right)x = 0 \tag{45}$$

which does not show a stiffening behaviour and, instead, predicts a critical value of the angular velocity for $\Omega = 1$, that is $\omega = \omega_0$, for which the oscillations grow without bound. This is in agreement with what has been observed with linear elastic multibody models (García-Vallejo et al., 2005a).

3.1. Approximate solutions based on the multiple time scale technique

The multiple time scales technique is a perturbation method in which different time scale can be used to avoid the presence of secular generating terms. It is based on a series expansion of the solution as follows

$$x(\tau,\epsilon) = x_0(T_0,T_1,T_2,\ldots) + \epsilon x_1(T_0,T_1,T_2,\ldots) + \epsilon^2 x_2(T_0,T_1,T_2,\ldots) + \ldots \tag{46}$$

where $T_j = \epsilon^j\tau$ (j = 0,1,2…) and ϵ is a small artificial parameter ($\epsilon << 1$).

In this section a second order solution is sought with the use of two time scales. This way, the non-dimensional variable x is expanded as follows

$$x(\tau,\epsilon) = x_0(T_0,T_1) + \epsilon x_1(T_0,T_1) + \mathcal{O}\left(\epsilon^2\right) \tag{47}$$

where $T_0 = \tau$ is the fast time scale and $T_1 = \epsilon\tau$ is the slow time scale. Due to the use of two time scales that depend on τ, the derivatives with respect to τ are carried out as follows

$$\frac{\mathrm{d}(\cdot)}{\mathrm{d}\tau} = \frac{\partial(\cdot)}{\partial T_0}\frac{\mathrm{d}T_0}{\mathrm{d}\tau} + \frac{\partial(\cdot)}{\partial T_1}\frac{\mathrm{d}T_1}{\mathrm{d}\tau} = \frac{\partial(\cdot)}{\partial T_0} + \frac{\partial(\cdot)}{\partial T_1}\epsilon = \mathrm{D}_0(\cdot) + \epsilon\mathrm{D}_1(\cdot) \tag{48}$$

$$\frac{\mathrm{d}^2(\cdot)}{\mathrm{d}\tau^2} = \frac{\partial\left(\mathrm{D}_0(\cdot) + \epsilon\mathrm{D}_1(\cdot)\right)}{\partial T_0} + \frac{\partial\left(\mathrm{D}_0(\cdot) + \epsilon\mathrm{D}_1(\cdot)\right)}{\partial T_1}\epsilon = \mathrm{D}_0^2(\cdot) + 2\epsilon\mathrm{D}_0\mathrm{D}_1(\cdot) + \mathcal{O}(\epsilon^2) \tag{49}$$

where $\mathrm{D}_{\mathrm{i}}^{\mathrm{k}}$ refers to

$$\mathrm{D}_{\mathrm{i}}^{\mathrm{k}} = \frac{\partial^{\mathrm{k}}(\cdot)}{\partial \mathrm{T}_{\mathrm{i}}^{\mathrm{k}}} \tag{50}$$

In order to solve the problem, the equation of motion has to be prepared by including the artificial parameter as follows

$$\ddot{x} + \omega_n^2 x = -\epsilon \left(g_1 x^3 + g_2 \left(x\dot{x}^2 + \ddot{x}x^2 \right) \right) \tag{51}$$

Substituting Eqs. (47), (48) and (49) into the nonlinear equation of motion and identifying terms with the same order in parameter ϵ, one may find the following equation for the first order solution (ϵ^0):

$$\mathrm{D}_0^2 \mathrm{x}_0 + \omega_{\mathrm{n}}^2 \mathrm{x}_0 = 0, \quad \mathrm{x}_0(0) = \mathrm{x}_0,\ \dot{\mathrm{x}}_0(0) = \dot{\mathrm{x}}_0 \tag{52}$$

where x_0 and $\dot{x}_0$ are the initial conditions. Consequently, the equation for the second order solution (ϵ^1) is:

$$\mathrm{D}_0^2 \mathrm{x}_1 + \omega_{\mathrm{n}}^2 \mathrm{x}_1 = -\left(\mathrm{g}_1 \mathrm{x}_0^3 + \mathrm{g}_2 \left(\mathrm{x}_0 \left(\mathrm{D}_0^1 \mathrm{x}_0 \right)^2 + \left(\mathrm{D}_0^2 \mathrm{x}_0 \right) \mathrm{x}_0^2 \right) \right) - 2\mathrm{D}_0 \mathrm{D}_1 \mathrm{x}_0, \quad \mathrm{x}_1(0) = 0,\ \dot{\mathrm{x}}_1(0) = 0 \tag{53}$$

The first order solution is a harmonic solution in which the coefficients may depend on T_1 as follows:

$$x_0(T_0, T_1) = A(T_1)\mathrm{e}^{j\omega_n T_0} + A^*(T_1)\mathrm{e}^{-j\omega_n T_0} \tag{54}$$

where j is the imaginary unit, $A(T_1) \in \mathbb{C}$ and $(\cdot)^*$ is the complex conjugate operator. The previous solution can be also expressed as

$$x_0(T_0, T_1) = \frac{1}{2} a(T_1)\mathrm{e}^{j\varphi(T_1)}\mathrm{e}^{j\omega_n T_0} + \frac{1}{2} a(T_1)\mathrm{e}^{-j\varphi(T_1)}\mathrm{e}^{-j\omega_n T_0} \tag{55}$$

where $a(T_1), \varphi(T_1) \in \mathbb{R}$ are real functions of the slow time scale T_1. Substituting Eq. (55) into Eq. (53), one may obtain the forced linear equation for the second order solution. The presence of resonant terms, those including a factor $\mathrm{e}^{\pm j\omega_n T_0}$, is avoided with the help of the two time scale, giving rise to the next solvability conditions:

$$a' = 0 \tag{56}$$

$$2.6638\Omega^2 a^3 + 0.2873 a^3 \omega_n^2 - 3.7913 a^3 + \varphi' a \omega_n = 0 \tag{57}$$

where the $(\cdot)'$ is used for a derivative with respect to T_1. The solutions of the previous differential equations in T_1 are

$$a = a_0 \tag{58}$$

$$\varphi = \varphi_0 - 0.2873 a_0^2 \omega_n T_1 + \left(3.7913 - 2.6638\Omega^2\right) \frac{a_0^2}{\omega_n} T_1 = \varphi_0 - \omega_n T_1 \left(\frac{3.3504\Omega^2 - 0.23963}{2.3901\Omega^2 + 12.362} \right) a_0^2 \tag{59}$$

where a_0 and φ_0 are constants that depend on the initial conditions.

Once the secular generating terms are eliminated, the equation for the order ϵ^2 can be written as

$$\mathrm{D}_0^2 \mathrm{x}_1 + \omega_{\mathrm{n}}^2 \mathrm{x}_1 = \mathrm{a}_0^3 \left(3.1492\Omega^2 + 4.5758\right) \cos\left(3\omega_{\mathrm{n}} \mathrm{T}_0 + 3\varphi(\mathrm{T}_1)\right) \tag{60}$$

which does not contain secular generating terms. The solution of the previous equation is

$$x_1 = \frac{1}{-8\omega_n^2} a_0^3 \left(3.1492\Omega^2 + 4.5758\right) \cos\left(3\omega_n T_0 + 3\varphi(T_1)\right) \tag{61}$$

Finally, turning back to 1 the artificial parameter ϵ, the full solution of the system is obtained as

$$x(\tau) = a_0 \cos\left(\omega_{NL}\tau + \varphi_0\right) - a_0^3 \frac{0.39365\Omega^2 + 0.57198}{2.3901\Omega^2 + 12.362} \cos\left(3\omega_{NL}\tau + 3\varphi_0\right) \tag{62}$$

where ω_{NL} is the nonlinear frequency of the system that can be expressed as follows

$$\omega_{NL} = \omega_n \left(1 - \left(\frac{3.3504\Omega^2 - 0.23963}{2.3901\Omega^2 + 12.362}\right) a_0^2\right) \tag{63}$$

The relation between the amplitude of the oscillations and the frequency ratio, Ω, is shown in Fig. 8 for different values of parameter Ω. It is interesting to see that the beam transits from hardening to softening as the frequency ratio, Ω, passes from 0 to ∞. The backbone curve for a $\Omega = 1$ is given for reference. Any value of Ω will give a backbone curve included in the shaded are of Fig. 8.

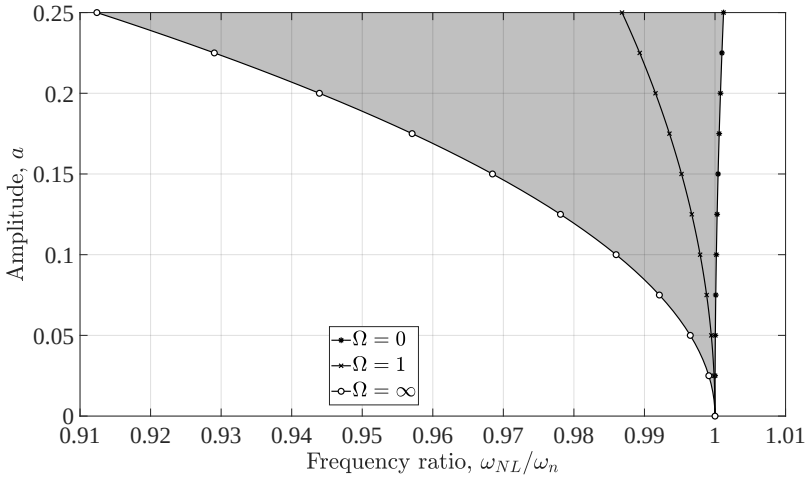

Figure 8: Relation amplitude to nonlinear frequency ratio (backbone curve) for different values of Ω.

To study the contribution of the nonlinear terms to the nonlinear natural frequency and to the nonlinear response $x(\tau)$, a pair of coefficients, $\lambda_\omega(\Omega)$ and $\lambda_x(\Omega)$, are defined so that

$$\omega_{NL} = \omega_n \left(1 - \lambda_\omega(\Omega)\, a_0^2\right) \quad \rightarrow \quad \lambda_\omega(\Omega) = \frac{3.3504\Omega^2 - 0.23963}{2.3901\Omega^2 + 12.362} \tag{64}$$

$$x(\tau) = a_0 \cos\left(\omega_{NL}\tau + \varphi_0\right) - a_0^3 \lambda_x(\Omega) \cos\left(3\omega_{NL}\tau + 3\varphi_0\right) \quad \rightarrow \quad \lambda_x(\Omega) = \frac{0.39365\Omega^2 + 0.57198}{2.3901\Omega^2 + 12.362} \tag{65}$$

Figure 9 shows how $\lambda_\omega(\Omega)$ and $\lambda_x(\Omega)$ vary with Ω. It can be seen that for low values of Ω the contribution of the nonlinear terms to the natural frequency and to the amplitude of the oscillations will be small. The influence of such terms will increase as the rotating velocity increases, but such influence is limited since both $\lambda_\omega(\Omega)$ and $\lambda_x(\Omega)$ tend to a constant value for large angular velocities. It must be said that the estimation provided by the analytical one-degree of freedom model presented before is not expected to be valid for large angular velocities where higher modes can be excited. Looking at the monotonic growth of coefficient $\lambda_\omega(\Omega)$ and $\lambda_x(\Omega)$, one can conclude that the effect of nonlinear terms changes monotonically from hardening at null angular velocity, see (Nayfeh et al., 1995), to softening at moderately high angular speed.

3.2. Approximations based on polynomial assumed shape functions

It is common to use polynomial functions with the assumed modes method (or Rayleigh's method) due to the ease of building polynomials that fulfil boundary conditions. In addition, polynomials can be expressed in terms of rational coefficients, what simplifies the application of the multiple time scales method, while they allow one to obtain closed expressions based on integer coefficients, which was impossible using the theoretical first mode shape of the cantilever beam as assumed shape function. For this reason, in this section the solutions obtained by using three different polynomial shape functions are given.

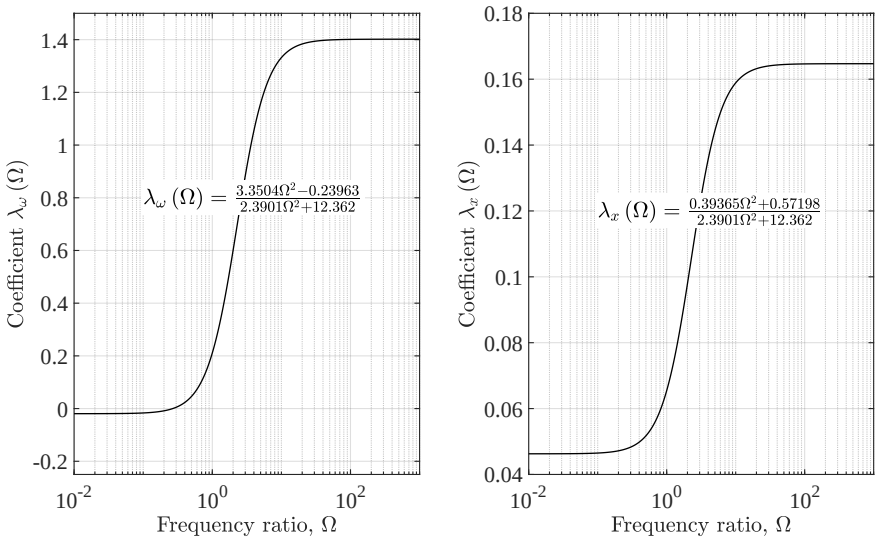

Figure 9: Left plot shows the evolution of λ_ω while right plot shows that of λ_x, both as a function of Ω.

Table 1
Characteristic values corresponding to the third degree polynomial shape function.

Parameter	Value
$\varphi_v(\eta)$	$\frac{3\eta^2}{2L^2} - \frac{\eta^3}{2L^3}$
$\varphi_u(\eta)$	$\frac{9\eta^4}{8L^5} - \frac{3\eta^3}{2L^4} - \frac{9\eta^5}{40L^6}$
ω_0	$\sqrt{\frac{140EI}{11L^3m}}$
ω_n^2	$\frac{350\Omega^2}{121} + \frac{140}{11}$
g_1	$\frac{144}{11} - \frac{9940\Omega^2}{1331}$
g_2	$\frac{142}{121}$
$\lambda_\omega(\Omega)$	$\frac{106855\Omega^2 - 34408}{84700\Omega^2 + 372680}$
$\lambda_x(\Omega)$	$\frac{52185\Omega^2 + 61424}{338800\Omega^2 + 1490720}$

Following the same approach described before, the functions and coefficients obtained when three polynomial shape functions are used are collected in Tables 1, 2 and 3. The results shown in Table 1 correspond to a third degree polynomial shape function that corresponds to the static deformation of a cantilever beam subject to a transverse tip load. The results shown in Table 2 corresponds to a fourth degree polynomial shape function that corresponds to the static deformation of a cantilever beam subject to uniformly distributed transverse load. Finally, the results shown in Table 3 corresponds to a fifth degree polynomial shape function that corresponds to the static deformation of a cantilever beam subject to a linearly distributed transverse load (zero force at the clamped end).

A comparison of the solutions obtained using the first theoretical mode of the cantilever beam and the three poly-

Table 2
Characteristic values corresponding to the fourth degree polynomial shape function.

Parameter	Value
$\varphi_v(\eta)$	$\frac{2\eta^2}{L^2} - \frac{4\eta^3}{3L^3} + \frac{\eta^4}{3L^4}$
$\varphi_u(\eta)$	$\frac{4\eta^4}{L^5} - \frac{8\eta^3}{3L^4} - \frac{8\eta^5}{3L^6} + \frac{8\eta^6}{9L^7} - \frac{8\eta^7}{63L^8}$
ω_0	$\sqrt{\frac{162EI}{13L^3m}}$
ω_n^2	$\frac{729\Omega^2}{338} + \frac{162}{13}$
g_1	$\frac{1296}{143} - \frac{1188\Omega^2}{169}$
g_2	$\frac{44}{39}$
$\lambda_\omega(\Omega)$	$\frac{5808\Omega^2 + 208}{3861\Omega^2 + 22308}$
$\lambda_x(\Omega)$	$\frac{1331\Omega^2 + 2132}{7722\Omega^2 + 44616}$

Table 3
Characteristic values corresponding to the fifth degree polynomial shape function.

Parameter	Value
$\varphi_v(\eta)$	$\frac{20\eta^2}{11L^2} - \frac{10\eta^3}{11L^3} + \frac{\eta^5}{11L^5}$
$\varphi_u(\eta)$	$\frac{300\eta^4}{121L^5} - \frac{800\eta^3}{363L^4} - \frac{90\eta^5}{121L^6} - \frac{100\eta^6}{363L^7} + \frac{150\eta^7}{847L^8} - \frac{25\eta^9}{2178L^{10}}$
ω_0	$\sqrt{\frac{32670EI}{2641L^3m}}$
ω_n^2	$\frac{32359635\Omega^2}{13949762} + \frac{32670}{2641}$
g_1	$\frac{40633500}{4154293} - \frac{828367611375\Omega^2}{117150101276}$
g_2	$\frac{55224507425}{48306119004}$
$\lambda_\omega(\Omega)$	$\frac{165450415265003000\Omega^2 - 660934414291675}{1157902503137780 4\Omega^2 + 61747006780148976}$
$\lambda_x(\Omega)$	$\frac{15442484235760175\Omega^2 + 23089508813459450}{92632200251022432\Omega^2 + 493976054241191808}$

nomial solutions presented in this section is shown in Fig. 10. Again, the mechanical properties of the model are a cross-sectional area of $7.299{\cdot}10^{-5}$ m^2, a second moment of the area of $8.214{\cdot}10^{-9}$ m^4, a Young modulus of $6.895{\cdot}10^{10}$ N/m^2, a mass density of 2767 kg/m^3 and a length of 8 m. Notice that the comparison is performed in terms of the spinning angular velocity, ω, since the different solutions obtained provide different values for ω_0. While the four models shows a similar trend, it is noticeable that the fifth order polynomial provides a better approximation to the solution based on the first theoretical mode for low frequencies. The reason is that the transverse deformation due to inertial force distribution is more similar to the static deformation due to linearly distributed forces than to the other two polynomial cases. Interestingly, no hardening behaviour is observed for the fourth order polynomial solution, which

is not consistent as shown by Nayfeh et al. (1995).

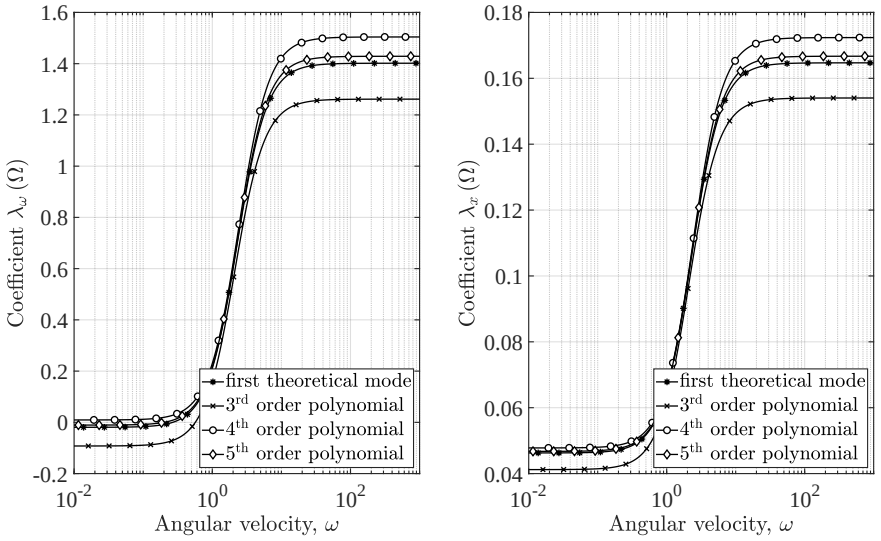

Figure 10: Left plot shows a comparison of λ_ω while right plot shows a comparison of λ_x for the three shape functions used as a function of ω.

4. Effect of the axial elongation due to centrifugal forces

In previous sections the beam was assumed to be inextensible. This helped at finding a simple model based only on a generalized coordinate that describes the transverse displacement of the beam tip during oscillations. However, comparing Fig. 8 to Fig. 5 reveals that the prediction of the frequency-amplitude relation of the analytical models is very different to the finite element results. In this section, the axial elongation of the beam due to centrifugal forces during steady rotation is included based on the following assumption. The axial displacement of an arbitrary point in the beam will be as follows:

$$u(\eta, t) = \varphi_u(\eta) q^2(t) + \Delta l(\eta) \tag{66}$$

where $\Delta l(\eta)$ is the axial displacement due to centrifugal forces. Notice that it is assumed that $\Delta l(\eta)$ does not depend on q, that is, does not depend on transverse vibration. This assumption is based on the fact the the axial deformation due to centrifugal forces arising from transverse vibration are much smaller than the global elongation due to the angular velocity of the rotating frame. In addition, since the rotating frame angular velocity, ω, is constant the centrifugal forces in the undeformed configuration would also be constant, producing a static axial deformation at the beam's tip of Δl_ω, whose value can be found by solving a static problem to be

$$\Delta l_\omega = \frac{m\omega^2 L^2}{3EA} \tag{67}$$

being m the beam's mass, E the Young modulus and A the cross-sectional area. Then, the displacement at an arbitrary point is evaluated using again the assumed mode method as

$$\Delta l(\eta) = \varphi_\omega(\eta) \Delta l_\omega \tag{68}$$

where $\varphi_\omega(\eta) = \sin\left(\frac{\pi\eta}{2L}\right)$ is the first mode of a cantilever beam in axial vibration. In what follows, it will be assumed that the axial displacement due to deformation, $\Delta l(\eta)$, has the same order as the axial displacement due to transverse deformation, $\varphi_u(\eta) q^2$, that is $\Delta l(\eta) \sim q^2$ and therefore $u \sim q^2$.

Due to the introduction of the axial elongation, the curvature approximation of Eq. (36) is no longer valid. Retaining terms of order q^4 in the approximation of κ^2, one can show now that

$$\kappa^2 = \left(\frac{\|\boldsymbol{r}'' \times \boldsymbol{r}'\|}{\|\boldsymbol{r}'\|^3} \right)^2 = \left(1 - 6\Delta l'(\eta)\right) \left(\varphi_v''(\eta) q\right)^2 + 2 \left(\varphi_v''(\eta) q\right)^2 \left(\varphi_u'(\eta) q^2 + \Delta l'(\eta)\right) - 2 \left(\varphi_v''(\eta) q\right) \left(\varphi_u''(\eta) q^2 + \Delta l''(\eta)\right) \left(\varphi_v'(\eta) q\right) + \mathcal{O}\left(q^6\right) \tag{69}$$

since

$$\left(\frac{1}{\|\boldsymbol{r}'\|^3} \right)^2 = 1 - 6\Delta l'(\eta) + \mathcal{O}\left(q^4\right) \tag{70}$$

where use has been made of the relation $2\varphi_u'(\eta) q^2 = -\left(\varphi_v'(\eta) q\right)^2$. Therefore, the bending elastic strain energy will be calculated as follows

$$V_b = \frac{1}{2} \int_0^L EI \left[\left(1 - 6\Delta l'(\eta)\right) \left(\varphi_v''(\eta) q\right)^2 + 2 \left(\varphi_v''(\eta) q\right)^2 \left(\varphi_u'(\eta) q^2 + \Delta l'(\eta)\right) - 2 \left(\varphi_v''(\eta) q\right) \left(\varphi_u''(\eta) q^2 + \Delta l''(\eta)\right) \left(\varphi_v'(\eta) q\right) \right] \mathrm{d}\eta + \mathcal{O}\left(q^6\right) \tag{71}$$

In addition, since the beam model is no longer inextensible, the longitudinal elastic strain energy must be included as follows

$$V_l = \frac{1}{2} \int_0^L EA \varepsilon_l^2 \mathrm{d}\eta \tag{72}$$

where ε_l is the Lagrangian definition of the longitudinal strain (Berzeri and Shabana, 2000), which reads as

$$\varepsilon_l = \frac{1}{2} \left(\|\boldsymbol{r}'\|^2 - 1 \right) \tag{73}$$

Retaining terms of order lower than q^8 in the approximation of ε_l^2, one can show that

$$\varepsilon_l^2 = \left(\Delta l'(\eta)\right)^2 + 2 \left(\varphi_u'(\eta) q^2\right) \left(\Delta l'(\eta)\right)^2 + \left(\varphi_u'(\eta) q^2\right)^2 \Delta l'(\eta) + \left(\Delta l'(\eta)\right)^3 + \mathcal{O}\left(q^8\right) \tag{74}$$

In the evaluation of the longitudinal elastic strain energy, one has to consider that

$$EA\Delta l'(\eta) = EA\varphi_\omega'(\eta) \frac{m\omega^2 L^2}{3EA} = \left(\frac{\varphi_\omega'(\eta) L^2}{3} \right) m\omega^2 \tag{75}$$

where $\varphi_\omega'(\eta) L^2/3$ is of order one. Therefore, the second and third terms at the right hand side of Eq. (74) will result in linear and cubic velocity dependent stiffness terms. The longitudinal elastic strain energy will be as follows

$$V_l = V_l^0 + \frac{m\omega^2 L^2}{6} \int_0^L \varphi_\omega'(\eta) \left(2 \left(\varphi_v'(\eta) q^2\right) \Delta l'(\eta) + \left(\varphi_u'(\eta) q^2\right)^2 \right) \mathrm{d}\eta + \mathcal{O}\left(q^6\right) \tag{76}$$

where V_l^0 is a constant term due to the first and fourth terms at the right hand side of Eq. (74) that will not contribute to the stiffness in the equation of motion. Finally, the total elastic strain energy will be $V = V_b + V_l$.

The consideration of the elongation obviously has an impact on the kinetic energy. The velocity of an arbitrary point in the beam cannot be evaluated through Eq. (30). Instead, the new velocity vector of an arbitrary point in the beam centre line reads now as follows:

$$\dot{\boldsymbol{r}} = \varphi_u(\eta) 2q\dot{q}\boldsymbol{i} + \left(\eta + \varphi_u(\eta) q^2 + \Delta l(\eta)\right) \omega \boldsymbol{j} + \varphi_v(\eta) \dot{q} \boldsymbol{j} - \varphi_v(\eta) q\omega \boldsymbol{i} \tag{77}$$

The consideration of the centrifugal elongation through function $\Delta l(\eta)$ requires the addition of a new nondimensional parameter, $\mu = I/(AL^2)$, which represents the slenderness of the beam. This is shown as follows

$$\Delta l(\eta) = \varphi_\omega(\eta) \frac{m\omega^2 L^2}{3EA} = \frac{1.8751^4}{3} \varphi_\omega(\eta) L \underbrace{\left(\frac{I}{AL^2} \right)}_{\mu} \Omega^2 \tag{78}$$

Table 4
Parameters of the nonlinear solution based on the first theoretical mode of the cantilever beam.

Parameter	Value
ω_0	$3.5160\sqrt{\frac{EI}{L^3 m}}$
ω_n^2	$12.987\Omega^4\mu - 254.89\Omega^2\mu + 2.3901\Omega^2 + 12.362$
g_1	$2.3785\Omega^2 + 10.110$
g_2	1.1492
$\lambda_\omega(\Omega)$	$\frac{3.7312\Omega^4\mu - 73.229\Omega^2\mu - 0.20528\Omega^2 - 0.23963}{12.987\Omega^4\mu - 254.89\Omega^2\mu + 2.3901\Omega^2 + 12.362}$
$\lambda_x(\Omega)$	$\frac{0.93280\Omega^4\mu - 18.307\Omega^2\mu + 0.097338\Omega^2 + 0.57198}{12.987\Omega^4\mu - 254.89\Omega^2\mu + 2.3901\Omega^2 + 12.362}$

where the first and last definitions of Eq. (40) have been used. For instance, in the case of a beam with a solid square cross-section of dimensions $b \times h$, the slenderness ratio μ reads as

$$\mu = \frac{\frac{bh^3}{12}}{bhL^2} = \frac{1}{12}\left(\frac{h}{L}\right)^2 \tag{79}$$

For the beam defined in Section 1, the slenderness ratio is $\mu = 1.7584\,10^{-6}$ and therefore, the contribution of the new terms affected by μ is expected to be small. By application of the multiple time scale technique, a nonlinear solution is found having the parameters collected in Table 4. By comparing the values of ω_n^2, g_1 and g_2 of the table with those of Eqs. (42)-(44), it can be observed that g_2 is the same in both cases, while ω_n^2 and g_1 have been modified. In the case of ω_n^2, the presence of terms that depend on the slenderness ratio, μ, and the non-dimensional angular velocity, Ω, is observed. In the case of the cubic term coefficient, g_1, the sign and magnitude of the velocity-dependent term have changed.

To evaluate the influence of the elongation on the nonlinear solution, the evolutions of coefficients $\lambda_\omega(\Omega)$ and $\lambda_x(\Omega)$ with Ω are shown in Fig. 11 for different values of μ. Comparing this figure with Fig. 9, one may see that the behaviour of the solution changes significantly. On one hand, both $\lambda_\omega(\Omega)$ and $\lambda_x(\Omega)$ start decreasing as Ω increases. According to the definition of $\lambda_\omega(\Omega)$ this results in an initial hardening with the angular velocity that may be significant depending on the slenderness ratio μ. Notice that this effect was not captured by the solution corresponding to Fig. 9. On the other hand, the maximum values achieved by $\lambda_\omega(\Omega)$ and $\lambda_x(\Omega)$ for high angular velocities are smaller than those of Fig. 9, what results in a less pronounced softening.

5. Accurate description of the shape function by using Frobenius approximation

So far, the first transverse vibration mode of a cantilever beam has been used as shape function to obtain the rotating beam model. Nevertheless, it is known that such mode does not coincide with the first mode of a rotating cantilever beam, in which the stiffness terms are dependent on the angular velocity. For this reason, this section obtains the first mode of a rotating cantilever beam to increase the precision of the mathematical model.

Since a closed form of the bending vibration modes of a rotating cantilever beam is not available, one needs to resort to approximation methods to achieve a good representation of the modes. As shown in Section 3.2, polynomial shape functions can be used to approximate complex modes. In 1982, Wright et al. (Wright et al., 1982) proposed a solution based on Frobenius method for solving partial differential equations. Their solution was proposed for tapered beams, but can be easily adapted to constant cross-section beams as explained next. Following their work, the following

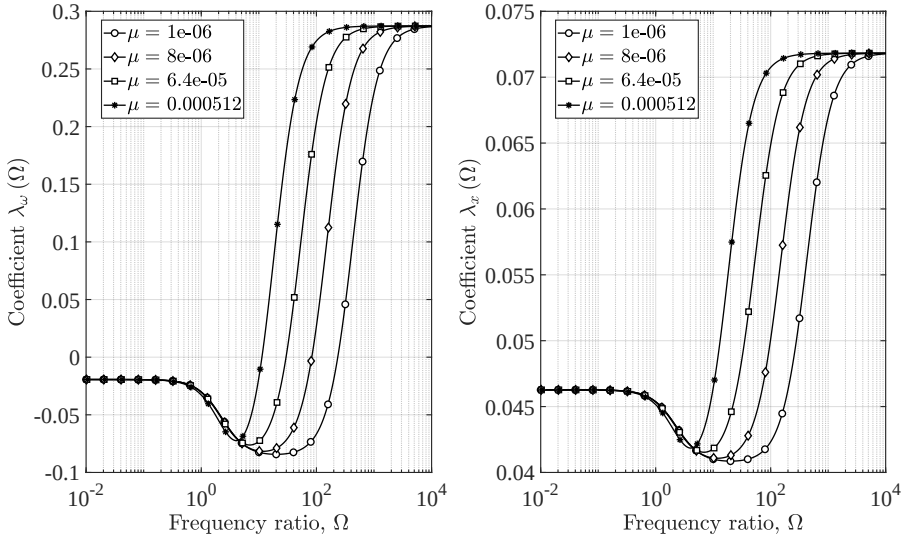

Figure 11: Left plot shows a the variation of λ_ω while right plot shows a variation of λ_x as a function of ω for different values of the slenderness ratio μ.

procedure has been used in this research. First, four independent polynomial are constructed as follows:

$$v_r(\eta) = \sum_{k=1}^{\infty} a_{r,k} \left(\frac{\eta}{L}\right)^k, \quad r = 0, 1, 2, 3. \tag{80}$$

where the polynomial coefficients a_{rk} are obtained using the following recursive formula:

$$a_{r,k} = \begin{cases} \frac{1}{2}\dfrac{\bar{\omega}^2}{k(k-1)} a_{r,k-2} - \frac{1}{2}\dfrac{\bar{\omega}^2(k-3)(k-4) - \bar{\omega}_n^2}{k(k-1)(k-2)(k-3)} a_{r,k-4} & \text{if} \quad k > r. \\ 1 & \text{if} \quad k = r. \\ 0 & \text{if} \quad k < r. \end{cases} \tag{81}$$

In the previous equation, $\bar{\omega}$ and $\bar{\omega}_n$ are the normalized spinning angular velocity and the normalized natural frequency, respectively, which read as follows:

$$\bar{\omega} = \frac{\omega}{\sqrt{\frac{EI}{mL^3}}}, \quad \bar{\omega}_n = \frac{\omega_n}{\sqrt{\frac{EI}{mL^3}}} \tag{82}$$

The procedure requires to solve an equation for $\bar{\omega}_n$ to be able to have an approximation of the mode shape. Once the four independent polynomial $v_r(\eta)$ have been built with a sufficiently high number of terms, the mode shape is obtained as a linear combination as follows:

$$\varphi_{Fr}(\eta) = C_0 v_0(\eta) + C_1 v_1(\eta) + C_2 v_2(\eta) + C_3 v_3(\eta) \tag{83}$$

where C_r ($r = 0, 1, 2, 3.$) are coefficients to be determined by using the mode shape boundary conditions. For a cantilever beam, one can show easily that $C_0 = C_1 = 0$ while

$$C_2 v_2''(L) + C_3 v_3''(L) = 0 \tag{84}$$

$$C_2 v_2'''(L) + C_3 v_3'''(L) = 0 \tag{85}$$

Since the mode shape cannot be null, the matrix of the previous homogeneous linear system must be rank deficient. This condition provides a polynomial equation that allows one to find the value of $\bar{\omega}_n$ given a certain spinning angular velocity $\bar{\omega}$, that is

$$f\left(\bar{\omega},\bar{\omega}_n\right)=\begin{vmatrix} v_2''(L) & v_3''(L) \\ v_2'''(L) & v_3'''(L) \end{vmatrix}=0 \tag{86}$$

Given a value of the angular velocity ω, one can use Eq. (86) to find an estimation of the natural frequency, ω_n. Using a large enough number of terms in the polynomial approximation, the estimation ω_n should converge to the exact value of the natural frequency. Fig. 12 shows how the estimation of the natural frequency, ω_n, converges to the exact value for different values of the angular velocity. It may be noted that the smaller the spinning angular velocity, the faster the convergence is. According to these results, the degree of the polynomial representation of the mode shape is fixed to 36.

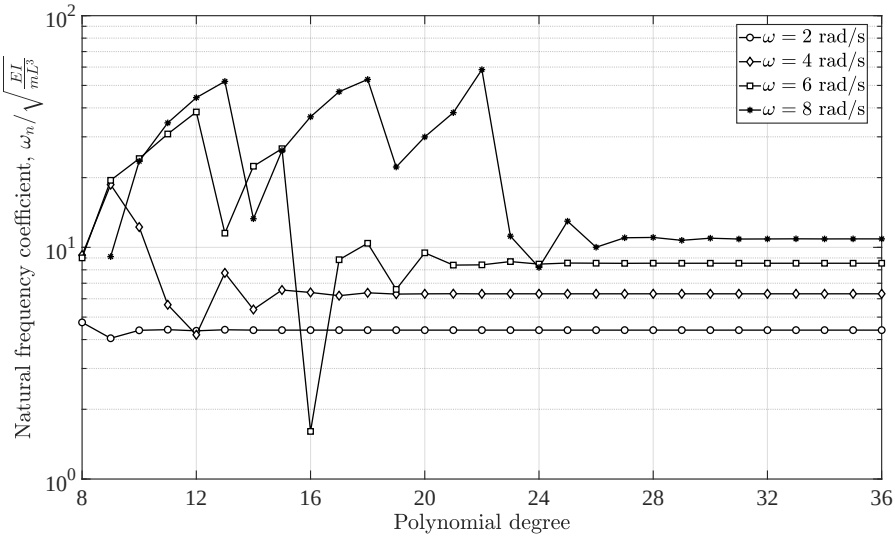

Figure 12: Convergence of the natural frequency estimation, ω_n, to the exact value for $\omega = 2, 4, 6, 8$ rad/s.

Once the value of the $\bar{\omega}_n$ has been obtained, one of the equations (85) is used to build the mode shape as follows:

$$\varphi_{Fr}(\eta)=C_3\left(-\frac{v_3''(L)}{v_2''(L)}v_2(\eta)+v_3(\eta)\right) \tag{87}$$

where the coefficient C_3 is selected to have $\varphi_{Fr}(L)=1$. Fig. 13 shows the first theoretical mode of a cantilever beam together with the converged approximations of the first mode shape of a rotating cantilever beam for four values of the angular velocity ($\omega = 2, 4, 6, 8$ rad/s). It is noticeable that the differences between the fixed cantilever beam mode shape and the rotating cantilever beam mode shape become significant as the angular velocity increases.

Since the presented procedure requires to solve numerically Eq. (86) for $\bar{\omega}_n$ prior to be able to build the mode shape, it will not be possible to obtain closed forms for the nonlinear solutions based on the multiple time scale technique applied to the model described in Section 4. Instead, one has to find a nonlinear solution for each value of the angular velocity. Table 5 shows four nonlinear solutions of the rotating beam problem using the mode shapes obtained with the Frobenius approximation method ($\varphi_{Fr}(\eta)$). While it is out of the scope of the present study, it is noteworthy that the multiple time scales method can also be applied directly to the beam's partial differential equations of motion, obtaining a zero-order problem that includes the centrifugal forces.

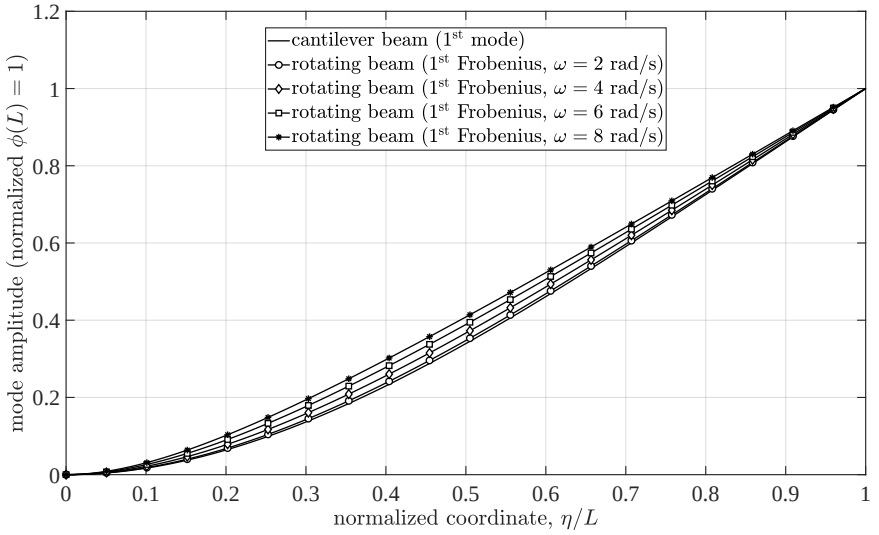

Figure 13: Comparison of the first mode shape of a fixed cantilever beam and that of a rotating cantilever beam for $\omega = 2, 4, 6, 8$ rad/s.

Table 5
Parameters of the nonlinear solutions obtained for $\omega = 2, 4, 6, 8$ rad/s.

ω [rad/s]	ω_n [rad/s]	$\lambda_\omega(\Omega)$	$\lambda_x(\Omega)$
2	3.03488	-0.0084683	0.046531
4	3.34565	0.010394	0.046761
6	3.73054	0.023546	0.046661
8	4.12419	0.030693	0.046445

6. Numerical analysis of the validity of the solution

In this section, the finite element model based on the Absolute Nodal Coordinate Formulation described in Section 2 has been used to generate numerical results to be compared with those provided by the simplified analytical model developed in this work. The index-3 differential algebraic equations of motion of the ANCF model, see for example (García de Jalon, J. and Bayo, E., 2012), have been integrated numerically using a second order implicit numerical integrator (trapezoidal rule) with a time step of $1.0{\cdot}10^{-3}$ s. The rheonomic constraints arising from the rotating clamped end have been stabilized during integration using Baumgarte's method (Baumgarte, 1972). After studying the mesh convergence, a model with 16 quadratic beam elements has been used. The total number of nodal coordinates of the model is 132, what leads to 130 degrees of freedom due to the addition of the 2 nonlinear constraints of Eq. (14). The total simulation time was fixed to 15 seconds, allowing to have in all analyzed cases at least five full cycles of steady oscillations that are used to compute the averaged amplitude and the averaged frequency. The numerical study is aimed at generating points of the backbone curve corresponding to different values of the spinning angular velocity. The amplitude of the steady nonlinear oscillations will increase as the acceleration time, T, of Eq. (1) is decreased. Therefore, to generate nonlinear oscillations with different amplitude levels, the acceleration time, T, of the numerical simulations will take the following values: 3.375 s, 3.25 s, 3 s, 2.75 s, 2.5 s and 2 s.

Figure 14 shows a comparison of the different solutions obtained in this work together with the finite element results described before. The solutions of the plot differ in the use or not of the assumption of inextensibility and the description of the deformation by the cantilever beam mode or by the Frobenius approximation for the rotating beam mode. The comparison has been shown for four different values of the spinning angular velocity ($\omega = 2, 4, 6, 8$ rad/s). It may be seen that the analytical solutions are very different to the real backbone curve obtained by the ANCF finite element model unless both elongation effect and Frobenius mode are used in the model. The agreement of the solution based on Frobenius approximation together with elongation consideration and the ANCF solution is reasonably good for moderately large amplitudes (deformations below 20 % of the beam's length) and for moderately large values of the spinning angular. As a reference, it must be said that an angular velocity of 8 rad/s approximately doubles the linear natural frequency of the rotating beam at such velocity ($\omega_n = 4.1242$ rad/s). Note that for larger values of the angular velocity, the contribution of higher modes is expected to be significant and the one-degree of freedom models presented here will not be valid any longer.

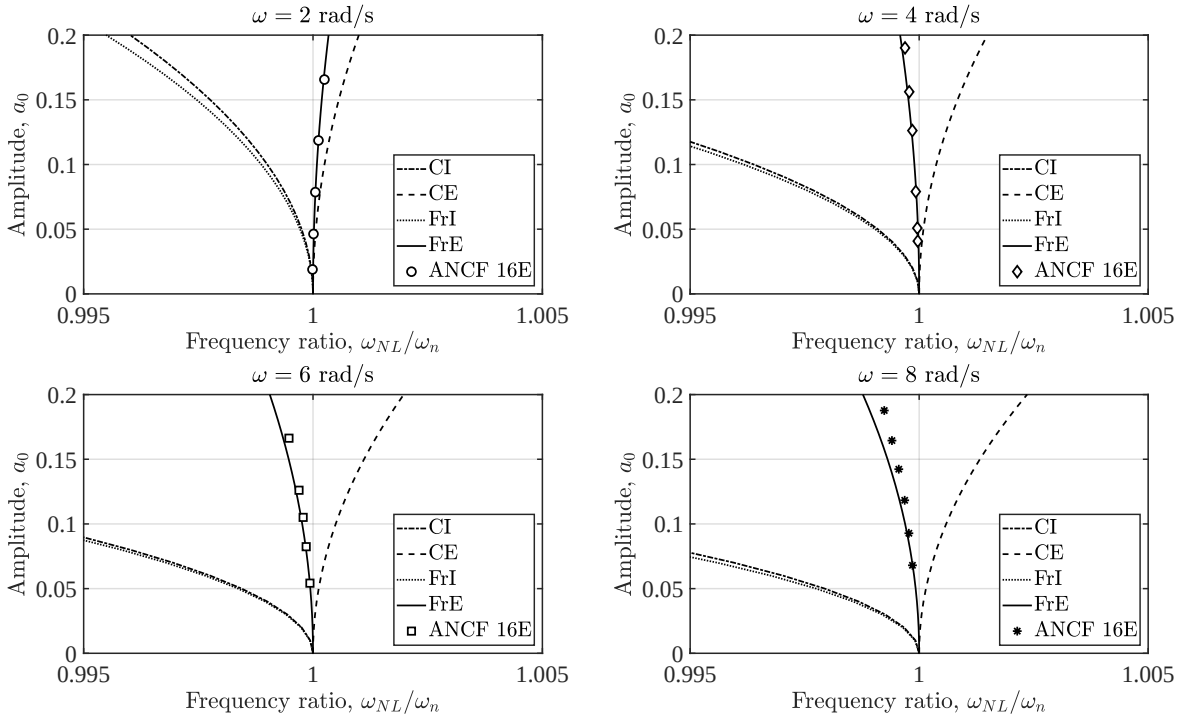

Figure 14: Comparison of the different solutions obtained for different $\omega = 2, 4, 6, 8$ rad/s. The acronyms CI, CE, FrI and FrE stand for the type of shape function and the use or not of the assumption of inextensibility (C = cantilever mode shape function, Fr = Frobenius approximation shape function, I = inextensible, E = extensible). The finite element results correspond to the acronym ANCF 16E.

According to Fig. 14, not considering the beam's extensibility results in overestimating the softening behaviour of the inertial terms. In addition, approximating the beam transverse deflection by the first transverse vibration mode of a cantilever beam instead of using the vibration mode of the rotating beam, here obtained using Frobenius approximation, results in overestimating the hardening.

The nonlinear solutions obtained for the different models developed have been compared to the results of the ANCF finite element model in Fig. 15 for a total time corresponding to one period of the finite element solution. The normalization of the state variables has been done as follows: $\bar{q} = q/L$, therefore $\bar{q}$ coincides with $x(\tau)$ in Eq. 62; and $\bar{\dot{q}} = \dot{q}/(\omega_0 L)$, where ω_0 is the first natural frequency of the beam for null spinning angular velocity (with cantilever boundary conditions). For the ANCF model q has been projected using Eq. (16). As shown in the figure, FrE's nonlinear multiple scales solution shows a better agreement with the ANCF solution than other solutions. It is interesting that solution FrI is noticeably close to the ANCF solution. However, due to the imprecise estimation

of the nonlinear natural frequency in this solution, the curve appears open since it shows a smaller nonlinear natural frequency. Both, CE and CI solutions are significantly inaccurate. The acronyms CI, CE, FrI and FrE stand for the type of shape function and the use or not of the assumption of inextensibility (C = cantilever mode shape function, Fr = Frobenius aproximation shape function, I = inextensible, E = extensible).

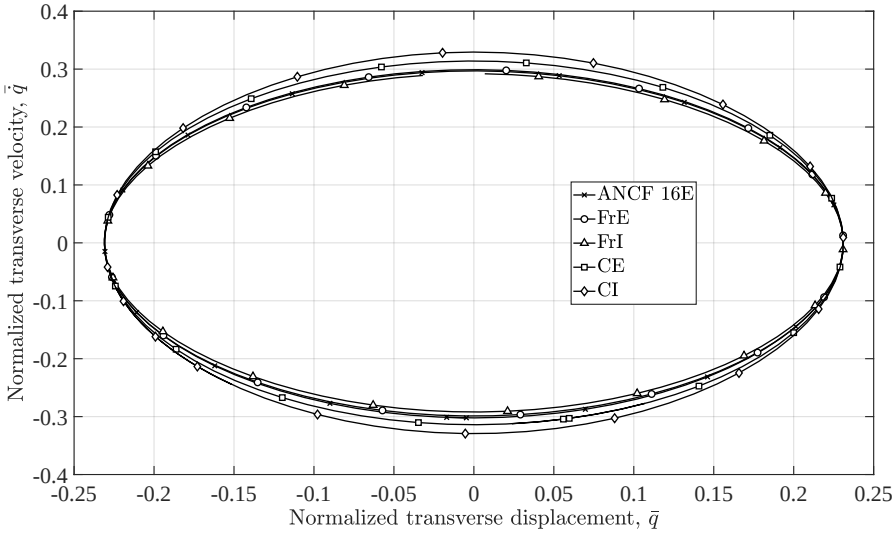

Figure 15: Phase space representation of the nonlinear oscillations for $\omega = 6$ rad/s. The ANCF finite element model has been discretized by using 16 quadratic elements, see Section 2. The acronyms CI, CE, FrI and FrE stand for the type of shape function and the use or not of the assumption of inextensibility (C = cantilever mode shape function, Fr = Frobenius aproximation shape function, I = inextensible, E = extensible).

7. Summary and conclusions

The nonlinear oscillations appearing in the steady motion of a rotating beam have been studied in this work through analytical and numerical results. A high-fidelity finite element model based on the absolute nodal coordinate formulation has been implemented and many simulations have been carried out in order to numerically obtain the backbone curves for different angular velocities. An analytical one-degree of freedom nonlinear model has been developed with the help of Lagrange equation. The nonlinearities of the analytical model are due to inertial and elastic forces. In the analytical model, starting from the geometrical definition of curvature only cubic nonlinearities have been retained. The influence of both the assumption of inextensibility and of the shape function definition used for the assumed-mode method have been investigated. To have a correct representation of the transverse vibration mode of the rotating beam, Frobenius method has been utilized.

Different solutions could be achieved using the multiple time scale perturbation method. The clear advantage of using the cantilever beam linear mode, or its polynomial approximations, is the possibility of having closed form expressions for the nonlinear response as a function of the angular velocity. Unfortunately, the approach based on Frobenius approximation required to obtain a nonlinear solution for each angular velocity. Nevertheless, the accuracy of the results of the Frobenius approximation model is remarkable as compared to the other shape functions used.

The results have shown that the consideration of the beam to be inextensible gives erroneous results for the estimation of the nonlinear natural frequency. In addition, this wrong estimation happens even if the transverse deformation is modelled through the use of an accurate representation of the linear transverse vibration mode of the rotating beam obtained by using Frobenius method. The results showed that approximating the beam transverse deflection by the first transverse vibration mode of a cantilever beam instead of using Frobeius approximation results in overestimating the hardening behaviour in the backbone curve.

Incorporating the extensibility by means of the static elongation caused by the centrifugal forces resulted in less inertial softening behaviour in the backbone curves. Only when the analytical model incorporated the exact representation of the rotating beam's first linear mode through Frobenius approximation and the extensibility due to centrifugal forces, its solution provided a reasonably approximated representation of the backbone curves as well as of the trajectories in the phase space. In addition, the rotating beam backbone curves show a transit from hardening at low spinning velocity to softening at high spinning velocity.

This work allowed to discuss the main effects that must be accounted for when generating simple models for the nonlinear oscillations of a rotating beam. Having closed-form nonlinear solutions like those proposed in this work might be useful for vibration control and design.

CRediT authorship contribution statement

González-Carbajal, J.: Conceptualization of this study, Methodology, Software. **Rincón-Casado, A.:** Conceptualization of this study, Methodology, Software. **García-Vallejo, D.:** Conceptualization of this study, Methodology, Software. **Domínguez, J.:** Conceptualization of this study, Methodology, Software.

References

Arvin, H., Arena, A., Lacarbonara, W., 2020. Nonlinear vibration analysis of rotating beams undergoing parametric instability: Lagging-axial motion. Mechanical Systems and Signal Processing 144. doi:10.1016/j.ymssp.2020.106892.

Atluri, S., 1973. Nonlinear vibrations of a hinged beam including nonlinear inertia effects. Journal of Applied Mechanics, Transactions ASME 40, 121–126. doi:10.1115/1.3422909.

Babilio, E., Lenci, S., 2017. On the notion of curvature and its mechanical meaning in a geometrically exact plane beam theory. International Journal of Mechanical Sciences 128-129, 277–293. doi:10.1016/j.ijmecsci.2017.03.031.

Banerjee, J., 2000. Free vibration of centrifugally stiffened uniform and tapered beams using the dynamic stiffness method. Journal of Sound and Vibration 233, 857–875. doi:10.1006/jsvi.1999.2855.

Banerjee, J., Jackson, D., 2013. Free vibration of a rotating tapered rayleigh beam: A dynamic stiffness method of solution. Computers and Structures 124, 11–20. doi:10.1016/j.compstruc.2012.11.010.

Banerjee, J., Kennedy, D., 2014. Dynamic stiffness method for inplane free vibration of rotating beams including coriolis effects. Journal of Sound and Vibration 333, 7299–7312. doi:10.1016/j.jsv.2014.08.019.

Baumgarte, J., 1972. Stabilization of constraints and integrals of motion in dynamical systems. Computer Methods in Applied Mechanics and Engineering 1, 1–16. doi:10.1016/0045-7825(72)90018-7.

Bekhoucha, F., Rechak, S., Duigou, L., Cadou, J., 2016. Nonlinear free vibrations of centrifugally stiffened uniform beams at high angular velocity. Journal of Sound and Vibration 379, 177–190. doi:10.1016/j.jsv.2016.05.045.

Berzeri, M., Shabana, A., 2000. Development of simple models for the elastic forces in the absolute nodal co-ordinate formulation. Journal of Sound and Vibration 235, 539–565. doi:10.1006/jsvi.1999.2935.

García de Jalon, J. and Bayo, E., 2012. Kinematic and Dynamic Simulation of Multibody Systems: The Real-Time Challenge. Mechanical Engineering Series, Springer New York.

García-Vallejo, D., Mikkola, A., Escalona, J., 2007. A new locking-free shear deformable finite element based on absolute nodal coordinates. Nonlinear Dynamics 50, 249–264. doi:10.1007/s11071-006-9155-4.

García-Vallejo, D., Sugiyama, H., Shabana, A., 2005a. Finite element analysis of the geometric stiffening effect. part 1: A correction in the floating frame of reference formulation. Proceedings of the Institution of Mechanical Engineers, Part K: Journal of Multi-body Dynamics 219, 187–202. doi:10.1243/146441905X10041.

García-Vallejo, D., Sugiyama, H., Shabana, A., 2005b. Finite element analysis of the geometric stiffening effect. part 2: Non-linear elasticity. Proceedings of the Institution of Mechanical Engineers, Part K: Journal of Multi-body Dynamics 219, 203–211. doi:10.1243/146441905X10050.

Hodges, D.H., 1979. Vibration and response of nonuniform rotating beams with discontinuities. Journal of the American Helicopter Society 24, 43–50.

Kim, H., Hee Yoo, H., Chung, J., 2013. Dynamic model for free vibration and response analysis of rotating beams. Journal of Sound and Vibration 332, 5917–5928. doi:10.1016/j.jsv.2013.06.004.

Kloda, L., Lenci, S., Warminski, J., 2018. Nonlinear dynamics of a planar beam–spring system: analytical and numerical approaches. Nonlinear Dynamics 94, 1721–1738. doi:10.1007/s11071-018-4452-2.

Lenci, S., Clementi, F., Rega, G., 2017. Comparing Nonlinear Free Vibrations of Timoshenko Beams with Mechanical or Geometric Curvature Definition, in: Procedia IUTAM, pp. 34–41. doi:10.1016/j.piutam.2017.03.006.

Lenci, S., Rega, G., 2016. Nonlinear Free Vibrations of Planar Elastic Beams: A Unified Treatment of Geometrical and Mechanical Effects, in: Procedia IUTAM, pp. 35–42. doi:10.1016/j.piutam.2016.03.007.

Mayo, J., Dominguez, J., Shabana, A., 1995. Geometrically nonlinear formulations of beams in flexible multibody dynamics. Journal of Vibration and Acoustics, Transactions of the ASME 117, 501–509. doi:10.1115/1.2874490.

Nayfeh, A., Chin, C., Nayfeh, S., 1995. Nonlinear normal modes of a cantilever beam. Journal of Vibration and Acoustics, Transactions of the ASME 117, 477–481. doi:10.1115/1.2874486.

Nayfeh, A., Nayfeh, S., 1994. On nonlinear modes of continuous systems. Journal of Vibration and Acoustics, Transactions of the ASME 116, 129–136. doi:10.1115/1.2930388.

Omar, M., Shabana, A., 2001. A two-dimensional shear deformable beam for large rotation and deformation problems. Journal of Sound and Vibration 243, 565–573.

Rajasekaran, S., 2013. Differential transformation and differential quadrature methods for centrifugally stiffened axially functionally graded tapered beams. International Journal of Mechanical Sciences 74, 15–31. doi:10.1016/j.ijmecsci.2013.04.004.

Rincón-Casado, A., González-Carbajal, J., García-Vallejo, D., Domínguez, J., 2021. Analytical and numerical study of the influence of different support types in the nonlinear vibrations of beams. European Journal of Mechanics, A/Solids 85. doi:10.1016/j.euromechsol.2020.104113.

Shabana, A., 2019. Vibration of Discrete and Continuous Systems. Mechanical Engineering Series, Springer International Publishing. doi:10.1007/978-3-030-04348-3.

Tang, A.Y., Li, X.F., Wu, J.X., Lee, K., 2015. Flapwise bending vibration of rotating tapered rayleigh cantilever beams. Journal of Constructional Steel Research 112, 1–9. doi:10.1016/j.jcsr.2015.04.010.

Thomsen, J.J., 2003. Vibrations and stability : advanced theory, analysis, and tools . 2nd ed. ed., Springer, Berlin.

Tian, J., Su, J., Zhou, K., Hua, H., 2018. A modified variational method for nonlinear vibration analysis of rotating beams including coriolis effects. Journal of Sound and Vibration 426, 258–277. doi:10.1016/j.jsv.2018.04.027.

Tsai, M., Lin, W., Zhou, Y., Hsiao, K., 2011. Investigation on steady state deformation and free vibration of a rotating inclined euler beam. International Journal of Mechanical Sciences 53, 1050–1068. doi:10.1016/j.ijmecsci.2011.08.011.

Valverde, J., García-Vallejo, D., 2009. Stability analysis of a substructured model of the rotating beam. Nonlinear Dynamics 55, 355–372. doi:10.1007/s11071-008-9369-8.

Warminski, J., Kloda, L., Lenci, S., 2020. Nonlinear vibrations of an extensional beam with tip mass in slewing motion. Meccanica 55, 2311–2335. doi:10.1007/s11012-020-01236-9.

Wright, A., Smith, C., Thresher, R., Wang, J., 1982. Vibration modes of centrifugally stiffened beams. Journal of Applied Mechanics, Transactions ASME 49, 197–202. doi:10.1115/1.3161966.

Zhang, B., Ding, H., Chen, L.Q., 2020. Three to one internal resonances of a pre-deformed rotating beam with quadratic and cubic nonlinearities. International Journal of Non-Linear Mechanics 126. doi:10.1016/j.ijnonlinmec.2020.103552.